Electron-phonon interaction and superconductivity in metallic molecular hydrogen. I. Electronic and dynamical properties under pressure

P. Cudazzo,[1] G. Profeta,[1] A. Sanna,[2,3,4] A. Floris,[3,4] A. Continenza,[1] S. Massidda,[2] and E. K. U. Gross[3,4]
[1]*CNISM, Dipartimento di Fisica, Università degli Studi dell'Aquila, Via Vetoio 10, Coppito, I-67010 L'Aquila, Italy*
[2]*CNR-IOM-SLACS and Dipartimento di Fisica, Università di Cagliari, I-09124 Monserrato, Cagliari, Italy*
[3]*Institut für Theoretische Physik, Freie Universität Berlin, Arnimallee 14, D-14195 Berlin, Germany*
[4]*European Theoretical Spectroscopy Facility (ETSF)*
(Received 7 January 2010; revised manuscript received 12 March 2010; published 2 April 2010)

The structural, electronic, and dynamical properties of molecular hydrogen under pressure are investigated by first-principles calculations. A detailed study of the *Cmca* phase, believed to be the stable phase at very high pressure, reveals the mechanisms of metallization and their impacts on the electronic and dynamical properties which are at the basis of the predicted onset of high-temperature superconductivity in molecular H_2. Pressure is shown to greatly affect the electronic and dynamical properties of this system acting on different and connected aspects, namely, Fermi surfaces, phonon softenings, charge transfer, all of them concurring as propitious features to the onset of high-temperature superconductivity.

DOI: 10.1103/PhysRevB.81.134505 PACS number(s): 74.62.Fj, 74.20.Pq, 74.25.Jb, 74.25.Kc

I. INTRODUCTION

The possibility of a superconducting phase in materials with light atomic constituents stimulated many researches in this field. The most illustrative example is the occurrence of superconductivity at high temperature in MgB_2 (Ref. 1) (transition temperature T_c of $\approx$40 K), a system with eight electrons per unit cell and with overlapping bands. Lithium under pressure [T_c as high as 15 K (Refs. 2–4)], boron[5] (T_c =11 K), silane,[6] and even-doped diamond,[7] are the most important and recent examples. However, the most intriguing and still puzzling system among the light elements under pressure is hydrogen. In its metallic form H was suggested to be a superconductor with high transition temperature both in monatomic and molecular phases.[8,9] Within a simple BCS theory, three fundamental properties concur to foresee high T_c in this system (and in general in light materials): (i) the small ionic mass guarantees large phonon frequencies that act as boson pairing field; (ii) the lack of electronic core, which screens out the electron-ion interaction, favors strong electron-phonon coupling; (iii) due to the large pressure needed to achieve the metallic molecular phase, metallic hydrogen is expected to exhibit wide electronic bands providing very efficient screening of the repulsive electron-electron Coulomb interaction.

However, despite all these considerations anticipating good perspectives for its superconducting properties, metallization of hydrogen is far from being obvious and easy to reach. In the search for metallic hydrogen, in fact, experiments found only three different insulating phases at pressures as large as 350 GPa:[10,11] at low temperature and low pressure ($P \leq 110$ GPa) hydrogen is stable as a rotational crystal with freely rotating molecules, whose centers of mass are arranged in a hexagonal-closed-packed lattice (phase I). At higher pressure (above 110 GPa) the quadrupole-quadrupole interaction freezes the librational (i.e., rotational) motion driving the system to the so called broken symmetry phase (phase II). This phase is stable up to 150 GPa where an additional phase transition occurs leading the system toward the so-called phase III. On the theoretical side, many works[12–14] based on density-functional theory (DFT), seem to agree that a stable molecular metallic phase of hydrogen exists on a pressure window between 400 and 500 GPa and that this phase is the *Cmca*, a layered structure with *ABAB* stacking belonging to the orthorhombic class. Above 500 GPa, the *Cmca* is believed to evolve toward a monatomic phase, characterized by the CsIV structure.[12–15] Due to the many technical difficulties at such elevated pressures, experimental evidences do not allow a conclusive determination of the crystal structure of phase II and III; thus, first-principles calculations acquire a fundamental role. Recently, Pickard and Needs[14] reported a completely *ab initio* phase diagram of H under high pressure up to 400 GPa considering many different phases, thus giving an extensive picture of the complex phase diagram of H_2 up to 400 GPa.

The interest in the metallization of hydrogen is always high, representing of the most elusive aspects of solid state physics. As a confirmation, very recently, interesting experimental and theoretical proposals to reach the metallization via alternative techniques[16,17]

Ashcroft[8,9] was the first to suggest possible superconductivity in H, pointing to some intriguing aspects peculiar to this system, such as the need for a consistent treatment of the electron-electron interaction. In a previous work, we investigated the possibility of a superconducting phase transition in molecular metallic hydrogen (*Cmca*) within DFT framework[18] and on the basis of density-functional theory extended to the superconducting state,[19] properly accounting for electron-phonon (el-ph) and electron-electron interaction. The study revealed that hydrogen presents high-T_c superconductivity with critical temperature values up to 242 K at 450 GPa. The high T_c was strictly related to the large el-ph coupling constant and to the occurrence of large phonon frequencies providing a wide energy range at the Fermi level (E_F) for electrons to interact through bosons exchange.

In this paper, extending on our previous work, we present a detailed study of the electronic and dynamical properties of molecular hydrogen under high pressure while an accurate

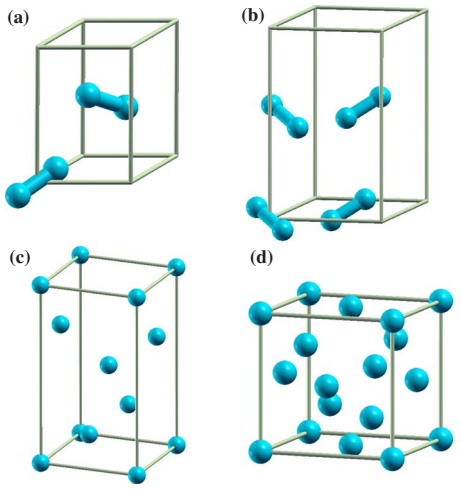

FIG. 1. (Color online) Different proposed structures for the metallic phase of hydrogen. Panel (a) *Cmca*; panel (b) $P2_1/c$; panel (c) CsIV; and panel (d) diamond phase.

analysis of the electron-phonon and electron-electron interactions and how they contribute to the overall superconducting properties is presented in Ref. 20. Here, we will show that the large electron-phonon coupling constant is related to the molecular nature of the system and to the particular metallization mechanism. In fact, while strong covalent bonds due to proton pairing give rise to large el-ph matrix elements, band-overlap metallization originates a complex Fermi surface (FS) characterized by many different and not-connected sheets, thus providing the basis for interband el-ph scattering processes involving a large number of electronic and phononic states. The paper is organized as follows: after a discussion of the computational details (Sec. II), we present in Sec. III an analysis of the phase diagram of H under pressure and of the *Cmca* phase. Then, we focus on electronic (Sec. IV) and dynamical properties (Sec. V) and finally draw our conclusions.

II. COMPUTATIONAL DETAILS

Our calculations are based on density-functional theory within local-density approximation [LDA (Ref. 21)] implemented in a pseudopotential plane-wave framework.[22] The *Cmca* phase has been simulated using a basis-centered orthorhombic (bco) lattice with two molecules per unit cell at ideal positions (0,0,0) and $(0,\frac{b}{2},\frac{c}{2})$, b and c being, respectively, along the y and z axes of the corresponding simple orthorhombic unit cell [Fig. 1 panel (a)]. In order to validate our computational accuracy, we considered other structures, namely, the $P2_1/c$ and the CsIV, which are considered to be competing with the *Cmca* in the pressure range of interest, taken as a simple orthorhombic and a body-centered tetragonal unit cells, respectively. In the case of the $P2_1/c$ we have a 4 molecules unit cell [with center of mass at (0, 0, 0), $(-\frac{a}{2},\frac{b}{2},0)$, $(0,\frac{b}{3},\frac{c}{2})$, $(-\frac{a}{2},\frac{5}{6}b,\frac{c}{2})$] while for the CsIV structure we have a 2 molecules unit cell [with center of mass at (0, 0, 0) and $(-\frac{a}{2},\frac{a}{4},\frac{c}{2})$]. We remark that these structures do not represent the complete phase diagram that indeed is much more complex:[14] these calculations are used only to assess the present computational accuracy.

At fixed volume, the optimized unit cells are obtained minimizing the total energy as a function of the structural parameters $(a,\frac{b}{a},\frac{c}{a})$; at each fixed value of the lattice parameters the atomic positions (i.e., the internal degrees of freedom) were fully relaxed to minimize the forces. The Bachelet *et al.*[23] pseudopotential is used: tests performed on the isolated H_2 molecule and on different molecular structures showed that a 60 Ry kinetic-energy cutoff is enough to achieve a well-converged basis set within 1 mRy in the total energy and 2% on the unit-cell structural parameters. Brillouin-zone (BZ) integration was performed using a $n\times n\times n$ Monkhorst-Pack[24] k-point mesh with $n=12$ for the *Cmca* and the diamond phase, $n=8$ for the $P2_1/c$ phase and $n=18$ for the CsIV. This choice, with a smearing of 0.02 Ry, gives convergence within about 2% on the structural parameters and 1 mRy on the total energy.

Phonon frequencies in the *Cmca* were calculated using the plane-waves method within linear-response theory[25] using a $26\times26\times26$ Monkhorst-Pack k-point mesh to compute the dynamical matrix. This allows us to achieve a very good convergence on the phonon spectrum (about 2% in the phonon frequencies). A $6\times6\times6$ q mesh in the first BZ was used to interpolate the force constants for the phonon-dispersion curve calculation.

III. STRUCTURAL PROPERTIES OF MOLECULAR METALLIC HYDROGEN AT HIGH PRESSURE

Given the complexity of the structural phase diagram of H_2 under pressure,[14] we concentrate on the *Cmca* phase, the most stable phase above 385 GPa (Ref. 14) found to be metallic by recent exact-exchange calculations.[13] However, in order to give an idea of the phase evolution of H_2 under pressure and to understand the main structural changes involved, we consider in the following some model structures predicted as possible competing stable structures of the molecular phase:[12] the $P2_1/c$, the *Cmca* and the CsIV phase which is the best candidate for the monatomic phase.[12–15] The unit cells of these structures are reported in Fig. 1 together with the diamond structure, often taken as reference structure. We concentrate on these three structures and investigate the phase diagram up to 500 GPa.

In Fig. 2 we show the behavior of the enthalpy as a function of pressure for the three phases considered at high pressure. We find that the $P2_1/c$ is the most stable up to $P=150$ GPa, where the system goes into the metallic *Cmca* phase. A recent computational study[14] investigated in great detail the complexity in this pressure range. In fact, above phase I the system is seen to go through the $C2/c$ phase (105–270 GPa) and the *Cmca*-12 phase (270–385 GPa), before reaching the *Cmca* phase. This latter is stable up to $P=490$ GPa, in agreement with our calculations, and is found to be metallic between 400 and 500 GPa.[12,13]

Being interested in the superconducting properties, we will concentrate on the pressure range selected for metallic molecular hydrogen[13,14] (i.e., 400–500 GPa) where the *Cmca*

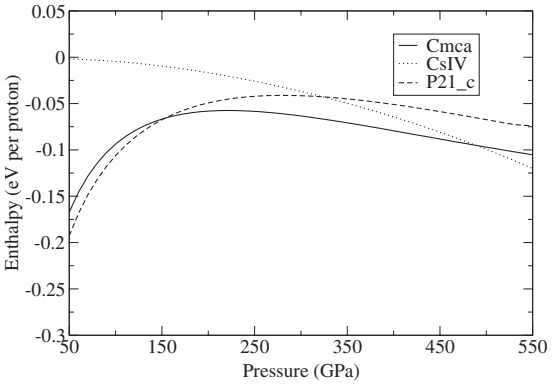

FIG. 2. Calculated enthalpy curves of the three phases considered here, referred to the monatomic diamond structure.

phase is stable, as found both by our calculated phase diagram and the more detailed study of Ref. 14.

The *Cmca* phase is a layered structure arranged in an *ABAB* stacking and can be represented as an orthorhombic unit cell with two molecules in the $z=0$ plane and two in the $z=c/2$ plane having opposite orientation with respect to the z axis. The same structure can be described using the bco unit cell shown in Fig. 3. The bco unit cell is characterized by three independent cell parameters: a, $\frac{b}{a}$, and $\frac{c}{a}$ with the optimized $\frac{b}{a}=\sqrt{3}$ in all the pressure range. As a consequence, the center of mass of the molecules lies on a hexagonal-close-packed lattice. The molecular axes form an angle θ with the xy plane which depends on the unit-cell parameters, while the azimuthal angle (i.e., the angle between the projection of the molecular axis on the xy plane and the x axis) takes the constant value $\phi=90°$. The total forces acting on the centers of mass of the two molecules in the bco unit cell are zero by

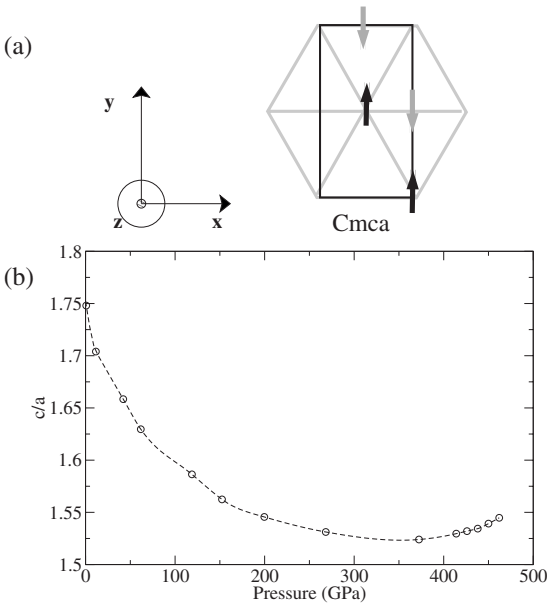

FIG. 3. Behavior of the c/a ratio in the bco unit cell as a function of pressure and schematic view of the *Cmca* phase with the orthorhombic (dashed line) and bco (continuous line) unit cell. Black (gray) arrows represent molecules at $z=0(z=c/2)$ plane and pointing toward the positive z hemisphere.

symmetry and the system has only two degrees of freedom: the angle θ and the intramolecular bond length (R) which, by symmetry, is the same for the two molecules. Although the centers of mass of the two molecules in the bco unit cell form a hcp lattice array at (0, 0, 0) and $(\frac{a}{2}, \frac{\sqrt{3}}{2}a, \frac{c}{2})$, the hexagonal symmetry is broken since molecules on different xy planes are inequivalent, being oriented in two different directions at angle θ and $2\pi-\theta$, respectively, with the xy plane (cf. Fig. 3, black and gray arrows).

In Fig. 3, the dependence of the cell parameters as a function of pressure is shown for the *Cmca* phase: we find that the c/a ratio is about 1.75 at $P=0$ GPa, larger than the ideal hcp value ($\sqrt{\frac{8}{3}}$). As pressure increases, c/a decreases to 1.54 at $P=438$ GPa, indicating that the system is more easily compressible along the z axis than in the xy plane: this suggests the presence of strong bonds localized in the xy plane, in line with the layered structure of the *Cmca* phase. Above 438 GPa the c/a begins to raise, showing that the intermolecular interaction between molecules on different layers increases and makes the interlayer bond stiffer. The angle θ (not shown) does not present a strong dependence on pressure: it increases between 0 and 462 GPa of about 10° while in the pressure region where the *Cmca* is stable it keeps values close to $\theta=30°$.

IV. ELECTRONIC PROPERTIES

The *Cmca* band structure and its behavior as a function of pressure (see Fig. 4) can be intuitively understood on a simple tight-binding basis considering bonding and antibonding combinations of H_2 molecular orbitals. At $P=0$ GPa [see Fig. 4 panel (a)], we may define intermolecular bonding and antibonding combinations of the two H_2 lower molecular orbitals and label them $\psi_{ij,\mathbf{k}}$, with energies $\epsilon_{ij,\mathbf{k}}$: here the indices $i,j=b,a$ define bonding and antibonding combinations, respectively, and their position as first and second index marks the intramolecular and intermolecular character, respectively (for example, $\psi_{ab,\mathbf{k}}$ is the wave function resulting from the bonding combination of antibonding molecular states). The overlap between molecular orbitals gives rise to four energy bands [see Fig. 4(a)]: the valence-band top is made of antibonding combination of intramolecular bonding orbitals $\psi_{ba,\mathbf{k}}$ while the conduction-band bottom is made of bonding combinations of intramolecular antibonding orbitals, $\psi_{ab,\mathbf{k}}$. The highest- and lowest-energy bands are made by $\psi_{aa,\mathbf{k}}$ and $\psi_{bb,\mathbf{k}}$-like states, respectively.

As the distance between molecules decreases, the larger overlap between molecular orbitals lowers the energy of the intermolecular bonding states with respect to the antibonding ones, pushing these latter toward higher energy. Both wave functions ($\psi_{ba,\mathbf{k}}$ and $\psi_{aa,\mathbf{k}}$), in fact, have nodes in the intermolecular region (cf. Fig. 5) and as pressure increases the repulsive electron-electron interaction is enhanced. As a result, the band gap progressively decreases with pressure: at about 40 GPa, within LDA, the bandwidth of bonding and antibonding states becomes larger than the splitting of the two molecular levels and the system goes into the metallic phase. Figure 5 shows the charge densities related to the four states $|\psi_{bb}|^2$, $|\psi_{ba}|^2$, $|\psi_{ab}|^2$, and $|\psi_{aa}|^2$ at the Γ point of the

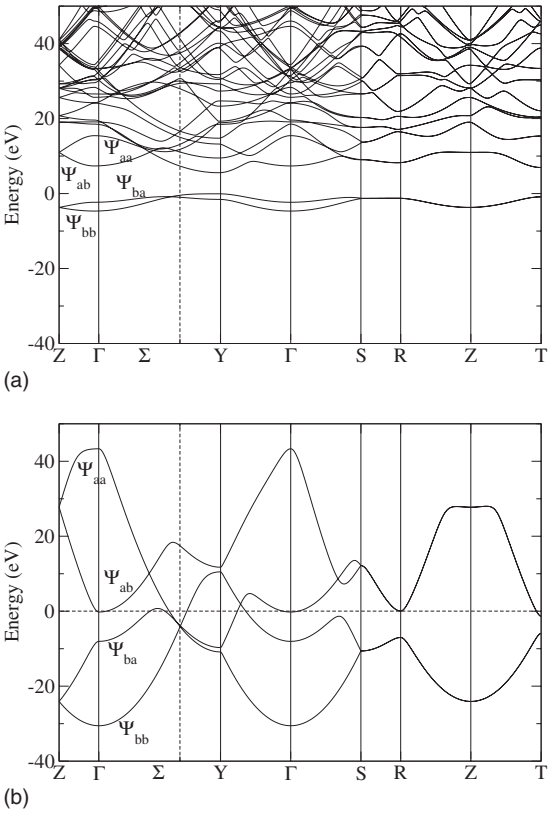

FIG. 4. Band structure of the *Cmca* phase at (a) $P=0$ and (b) $P=414$ GPa.

irreducible BZ (IBZ). The states $\psi_{bb,\mathbf{k}}$ and $\psi_{ba,\mathbf{k}}$ are localized on layers within the xy planes and are responsible for the intramolecular and the in-plane intermolecular bonds, this latter being mainly contributed by the $\psi_{bb,\mathbf{k}}$ state.

Both $\psi_{ab,\mathbf{k}}$ and $\psi_{aa,\mathbf{k}}$ states show antibonding molecular character with charge distribution localized in the interlayer region and thus are responsible for the bond between molecules in the unit cell. In Fig. 6 panel (a) the band structure of the *Cmca* phase is shown at two different pressure values: $P=414$ GPa and $P=462$ GPa. We can distinguish three bands crossing the Fermi level ($\epsilon_{ba,\mathbf{k}}$, $\epsilon_{ab,\mathbf{k}}$, and $\epsilon_{aa,\mathbf{k}}$) while the bonding state $\psi_{bb,\mathbf{k}}$ is always completely filled, granting the stability of each H_2 unit over all the pressure range.

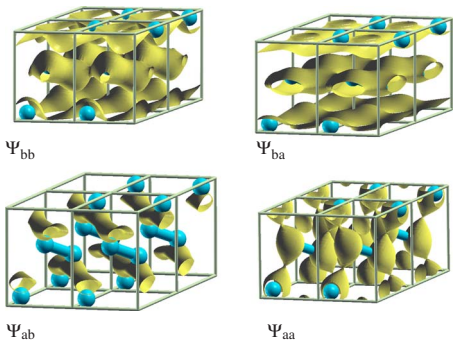

FIG. 5. (Color online) Three-dimensional contour plots of the bonding and antibonding charge densities at the Γ point of the first Brillouin zone at $P=414$ GPa.

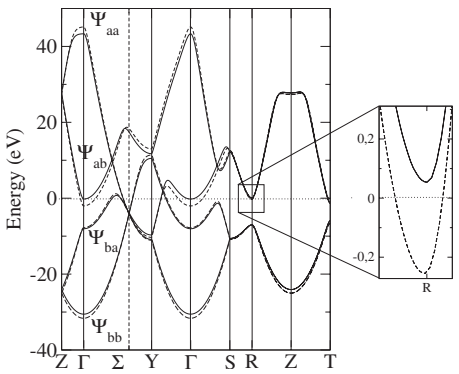

FIG. 6. Band structure of the *Cmca* phase at 414 and 462 GPa, solid and dashed line, respectively.

Metallization induces a charge transfer from bonding to antibonding states and some charge is displaced from the intralayer toward the interlayer regions leading to the formation of interlayer bonds, which are completely lacking in the insulating phase. At larger pressure, the overlap between bonding and antibonding molecular states ($\epsilon_{ba,\mathbf{k}}, \epsilon_{ab,\mathbf{k}}$) increases, weakening the intramolecular bond and the stability of the H_2 unit, and eventually leading to the monatomic metallic phase. This is clearly illustrated in Fig. 6, where we see that the band $\epsilon_{ba,\mathbf{k}}$ raises over E_F while the bands at higher energy (e.g., $\epsilon_{ab,\mathbf{k}}$) are pushed below the Fermi level in a few regions of the Brillouin zone (see the R and Γ points as examples). This energy order inversion of some of the bands has immediate consequences on the orbitals populations: as pressure increases, charge is transferred from the intramolecular toward the intermolecular region. In addition, since the symmetry of the wave functions is reduced away from the zone center, some of the intermolecular antibonding states can gain intermolecular bonding character thus further lowering their energy. This occurs, for example, to the $\psi_{aa,\mathbf{k}}$ state near the T point (degenerate in energy with the state $\psi_{ab,\mathbf{k}}$) or along the Σ line where the band $\epsilon_{aa,\mathbf{k}}$ drops below E_F.

In its metallic phase, hydrogen can be considered as a semimetal: the Fermi level E_F is pinned to a local minimum of the density of states (DOS) (see Fig. 7) separating bonding from antibonding states, a characteristic of the insulating phase. As shown in Fig. 7, the DOS at E_F raises with pressure: since the hopping terms increase with pressure, the two peaks below and above E_F widen and necessarily lead to an increasing DOS at the local minimum with pressure.

The FS (see Fig. 8) of the metallic phase under pressure is particularly reach and complex due to the several energy bands crossing E_F. In Fig. 8, we show a plot of the FS at the same pressures considered for the band structure. There are essentially three types of structures which are kept almost constant under pressure while at higher pressure some new surface portions appear. We can distinguish two tubular structures that cut the k_y axis and two "prismlike" structures parallel to k_x: all these structures are related to $\epsilon_{ba,\mathbf{k}}$ and have holelike character; the rounded region (disk) centered at Γ and the large structures lying along k_x direction at the edges of IBZ are formed by the $\epsilon_{ab,\mathbf{k}}$ state and have electronlike character. Finally, the other sheets are intersections of the

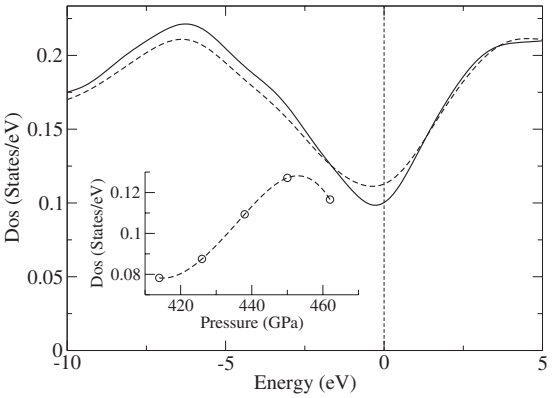

FIG. 7. Density of states of the *Cmca* phase at 414 and 462 GPa, solid and dashed line, respectively. Inset: density of states at E_F as a function of pressure.

$\epsilon_{aa,\mathbf{k}}$ and $\epsilon_{ab,\mathbf{k}}$ orbitals. We observe that between 426 and 438 GPa, the bands $\epsilon_{ab,\mathbf{k}}$ and $\epsilon_{aa,\mathbf{k}}$ drop below E_F [see Fig. 4(a)] originating four new structures at the edges of IBZ in the $z = \frac{\pi}{c}$ plane [see Fig. 8(b)]. As we will discuss in Ref. 20, these new FS sheets will be very important for superconductivity. To summarize, the *Cmca* phase at high pressure presents three bands crossing E_F: one of them has hole-type character and is related to intramolecular bonding states, the others are electron-type bands and are due to intramolecular antibonding states. Hole-type bands have a charge distribution localized in the *xy* planes, responsible for both the intramolecular and the intermolecular bond on the same layer. Electron-type bands, on the other hand, are characterized by a charge distribution localized in the interlayer regions and are responsible for interlayer bonds. Applied pressure induces a progressive charge transfer from bonding to antibonding states, that is, from intralayer to interlayer regions.

V. DYNAMICAL PROPERTIES

The molecular nature of the system greatly affects its dynamical properties as well, giving rise to different types of vibrations well separated in energy: namely, *phonons*, *librons*, and *vibrons*. Figures 9(a) and 9(b) show the phonon spectra along selected symmetry lines in the IBZ calculated within linear-response theory.[25] Considering an ideal system made of two isolated molecules, we would expect 6 modes

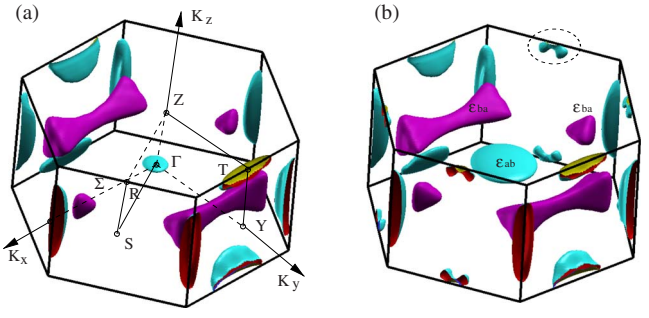

FIG. 8. (Color online) Fermi surface at (a) $P=414$ GPa and (b) $P=462$ GPa.

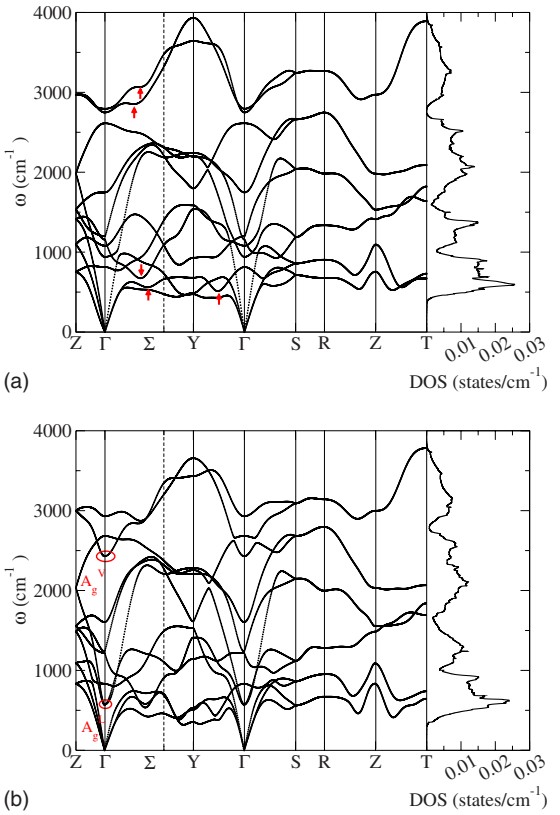

FIG. 9. (Color online) Phonon spectra of the *Cmca* phase at (a) $P=414$ GPa and (b) $P=462$ GPa. Arrows on panel (a) indicate some phonon anomalies.

related to the motion of the centers of mass of the two units, 4 modes related to the rotational motion (2 for each molecule), and 2 modes related to the vibrational motion (1 for each molecule).

In the condensed phase, the centers-of-mass motion gives rise to three acousticlike and three opticlike modes (*phonon* modes) involving displacements of the center of mass of the molecules that keep fixed the intramolecular bond length and the molecular axis orientation. While these modes are essentially decoupled from the internal motions, the other modes (i.e., rotational and vibrational) are not completely separated since, due to intermolecular interactions, a pure rotation is not allowed in a crystal. Therefore, the rotational degrees of freedom originate four *libronic* modes characterized by displacements perpendicular to the molecular axis involving a rotation and a simultaneous stretch of each single molecule. On the other hand, vibrational modes give rise to two *vibronic* modes characterized by displacements along the molecular axis.

The energies of the phonon modes at the zone center for $P=414$ and $P=462$ GPa are listed in Table I, while the complete phonon dispersions are shown in Fig. 9 with the corresponding densities of states.

A more detailed analysis of the phononic density of states (Fig. 9) reveals three principal regions in the phononic spectra: (i) a lower-frequency region ($0 \leq \omega \leq 1600$ cm^{-1}) separated by a pseudogap from the next region, is characterized by three acousticlike phononic modes, one opticlike

TABLE I. Phonon modes at Γ point at two different pressures, labeled according to their symmetry and phonon character.

Symmetry	$\omega(\Gamma)$ (cm^{-1}) $P=414$ GPa	$\omega(\Gamma)$ (cm^{-1}) $P=462$ GPa	Character
B_{1u}	0	0	Phononic
B_{2u}	0	0	Phononic
B_{3u}	0	0	Phononic
B_{1u}	811	835	Phononic
A_g	945	570	Libronic
B_{1u}	1065	570	Libronic
B_{3g}	1160	1206	Libronic
A_u	1200	1206	Phononic
B_{2g}	1750	1600	Libronic
B_{2u}	2610	2675	Phononic
B_{3g}	2745	2928	Vibronic
A_g	2793	2430	Vibronic

phononic mode along the *y* axis, and three libronic modes at small wave vectors; (ii) an intermediate frequency region ($1600 \leq \omega \leq 2700$ cm^{-1}) with libronic modes at large **q** and optical modes the along *x* and *z* axes; (iii) a high-frequency region related to the vibronic modes. The presence of a gap at about 2700 cm^{-1} in the frequency spectrum shows that the center-of-mass (i.e., phononlike) motion is effectively decoupled from intramolecular (i.e., vibronlike) motion. This assures that up to 414 GPa the paired molecular state still persists. The phonon density of states does not show remarkable changes in the pressure range considered (see Fig. 9): the main features are preserved and only a small shift toward lower frequencies can be observed in the topmost part of the phononic spectrum.

As can be noticed in Fig. 9(a) and from Table I, many phonon frequency softenings occur: in particular, at 414 GPa, we point out the high-frequencies vibronic modes (A_g) dropping from about 4000 cm^{-1} at *Y* point of the IBZ to about 3000 cm^{-1} close to Γ, and the libronic modes in the *yz* plane (A_g) from 2000 at Z to 1000 cm^{-1} at Γ. Other anomalies [see arrows in Fig. 9(a)] are present both along the Σ line (the B_{2u} acoustic mode, the B_{3g} libronic mode and the vibronic modes, in increasing energy order) and along the YΓ line, the B_{1u} phononic mode. While the anomalies along the Σ and YΓ lines are not sensitive to pressure. The nesting function shows peaks at the q's along the Σ and Y-G lines, suggesting that the observed anomalies along these lines are pure Kohn anomalies. Otherwise, the softening of the libronic and vibronic modes (with pressure) point toward possible strong (and increasing with pressure) el-ph coupling, as confirmed by the calculation of the el-ph coupling.[20]

VI. CONCLUSIONS

We presented a detailed study of the structural, electronic, and dynamical properties of the *Cmca* phase of hydrogen, the stable molecular phase at high pressure. Our study points out all the peculiarities of the molecular phase and of the metallization process which turns out to play a key role on the superconducting phase. In particular we find: (i) a complex Fermi surface made of several sheets with very different orbital character; (ii) low as well as high-frequency phonon modes that couple with electronic states producing a charge sloshing between bonding and antibonding states weakening (strengthening) intramolecular (intermolecular) bonds; (iii) a large effect of pressure on both electronic and dynamical properties, i.e., increase in band overlap, formation of new FS sheets, nontrivial phonon frequency variations. (iv) We found three different frequencies regions related to intermolecular translations modes, librational modes, and intramolecular modes, practically separated in energy. We found softening of many modes with increasing pressure.

ACKNOWLEDGMENTS

We acknowledge support from INFM-CNR through Inizziativa di Calcolo Parallelo. Work partially supported by the Italian Ministry of Education, through PRIN 2008XWLWF9_003 project and supercomputing grant at Cineca (Bologna, Italy).

[1] J. Nagamatsu, N. Nakagawa, T. Muranaka, Y. Zenitani, and J. Akimitsu, Nature (London) **410**, 63 (2001).
[2] K. Shimizu, H. Ishikawa, D. Takao, T. Yagi, and K. Amaya, Nature (London) **419**, 597 (2002).
[3] V. V. Struzhkin, M. I. Eremets, W. Gan, H.-K. Mao, and R. J. Hemley, Science **298**, 1213 (2002).
[4] S. Deemyad and J. S. Schilling, Phys. Rev. Lett. **91**, 167001 (2003).
[5] M. I. Eremets, V. V. Struzkhin, H. Mao, and R. J. Hemley, Science **293**, 272 (2001).
[6] M. I. Eremets, I. A. Trojan, S. A. Medvedev, J. S. Tse, and Y. Yao, Science **319**, 1506 (2008).
[7] E. A. Ekimov, V. A. Sidorov, E. D. Bauer, N. N. Mel'nik, N. J. Curro, J. D. Thompson, and S. M. Stishov, Nature (London) **428**, 542 (2004).
[8] N. W. Ashcroft, Phys. Rev. Lett. **21**, 1748 (1968).81
[9] C. F. Richardson and N. W. Ashcroft, Phys. Rev. Lett. **78**, 118 (1997).
[10] C. Narayana, H. Luo, J. Orloff, and A. L. Ruoff, Nature (London) **393**, 46 (1998).
[11] P. Loubeyre, F. Occelli, and R. LeToullec, Nature (London) **416**, 613 (2002).
[12] K. Johnson and N. W. Ashcroft, Nature (London) **403**, 632 (2000).
[13] M. Städele and R. M. Martin, Phys. Rev. Lett. **84**, 6070 (2000).
[14] C. J. Pickard and R. Needs, Nat. Phys. **3**, 473 (2007).

[15] V. Natoli, R. M. Martin, and D. M. Ceperley, Phys. Rev. Lett. **70**, 1952 (1993).
[16] I. Tamblyn and S. A. Bonev, Phys. Rev. Lett. **104**, 065702 (2010).
[17] X. J. Chen, V. V. Struzhkin, Y. Song, A. F. Goncharov, M. Ahart, Z. Liu, H.-k. Mao, and R. J. Hemley, Proc. Natl. Acad. Sci. U.S.A. **105**, 20 (2008).
[18] L. Zhang, Y. Niu, Q. Li, T. Cui, Y. Wang, Y. Ma, Z. He, and G. Zou, Solid State Commun. **141**, 610 (2007).
[19] P. Cudazzo, G. Profeta, A. Sanna, A. Floris, A. Continenza, S. Massidda, and E. K. U. Gross, Phys. Rev. Lett. **100**, 257001 (2008).
[20] P. Cudazzo *et al.* Phys. Rev. B. **81** 134506 (2010).
[21] J. P. Perdew and A. Zunger, Phys. Rev. B **23**, 5048 (1981).
[22] P. Giannozzi, S. Baroni, N. Bonini, M. Calandra, R. Car, C. Cavazzoni, D. Ceresoli, G. L. Chiarotti, M. Cococcioni, I. Dabo, A. Dal Corso, S. de Gironcoli, S. Fabris, G. Fratesi, R. Gebauer, U. Gerstmann, C. Gougoussis, A. Kokalj, M. Lazzeri, L. Martin-Samos, N. Marzari, F. Mauri, R. Mazzarello, S. Paolini, A. Pasquarello, L. Paulatto, C. Sbraccia, S. Scandolo, G. Sclauzero, A. P. Seitsonen, A. Smogunov, P. Umari, and R. M. Wentzcovitch, J. Phys.: Condens. Matter **21**, 395502 (2009).
[23] G. B. Bachelet, D. R. Hamann, and M. Schlüter, Phys. Rev. B **26**, 4199 (1982).
[24] H. J. Monkhorst and J. D. Pack, Phys. Rev. B **13**, 5188 (1976).
[25] P. Giannozzi, S. de Gironcoli, P. Pavone, and S. Baroni, Phys. Rev. B **43**, 7231 (1991).